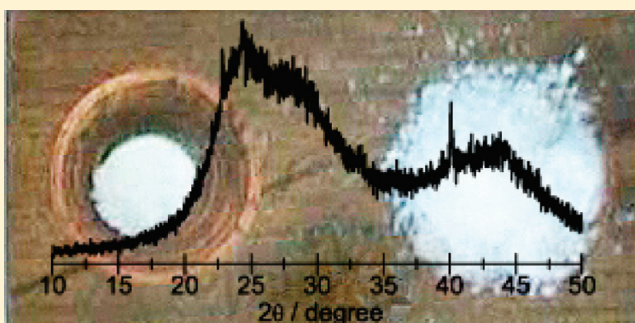


# Equilibrated High-Density Amorphous Ice and Its First-Order Transition to the Low-Density Form

Katrin Winkel,<sup>\*,†,‡</sup> Erwin Mayer,<sup>†,§</sup> and Thomas Loerting<sup>‡</sup><sup>†</sup>Institute of General, Inorganic and Theoretical Chemistry and <sup>‡</sup>Institute of Physical Chemistry, University of Innsbruck, Innrain 52a, A-6020 Innsbruck, Austria Supporting Information

**ABSTRACT:** We investigate the downstroke transition from high- (HDA) to low-density amorphous ice (LDA) at 140 (H<sub>2</sub>O) and 143 K (D<sub>2</sub>O). The visual observation of sudden phase separation at 0.07 GPa is evidence of the first-order character of the transition. Powder X-ray diffractograms recorded on chips recovered from the propagating front show a double halo peak indicative of the simultaneous presence of LDA and HDA. By contrast, chips picked from different parts of the sample cylinder show either HDA or LDA. Growth of the low-density form takes place randomly somewhere inside of the high-density matrix. The thermal stability of HDA against transformation to LDA at ambient pressure significantly increases with decreasing recovery pressure and reaches its maximum at 0.07 GPa. A sample decompressed to 0.07 GPa is by  $\sim 17$  K more stable than an unannealed HDA sample. An increasingly relaxed nature of the sample is also evident from the progressive disappearance of the broad calorimetric relaxation exotherm, preceding the sharp transition to LDA. Finally, we show that two independent thermodynamic paths lead to a very similar state of (relaxed) HDA at 140 K and 0.2 GPa. We argue that these observations imply an equilibrated nature of the amorphous sample in the pressure range of  $p \lesssim 0.2$  GPa and speculate that the observation of macroscopic phase separation involves two ultraviscous liquid phases at 140 K. This supports the scenario of a first-order liquid–liquid transition in bulk water.



## INTRODUCTION

First-order liquid–liquid phase transitions in single-component systems are a relatively new concept in thermodynamics.<sup>1</sup> The existence of such transitions would be helpful in explaining properties of anomalous liquids such as water.<sup>2–5</sup> However, until now, it has not been clear whether these transitions can indeed be observed in molecular bulk liquids. First-order-like transitions have been reported from one amorphous state of water to a structurally distinct amorphous state (“polymorphic transition”)<sup>6–11</sup> but challenged in subsequent studies.<sup>12–16</sup> It remained speculative whether these low-temperature, nonequilibrium transitions are pendants to equilibrium liquid–liquid transitions at higher temperatures<sup>17</sup> because it has been difficult to clearly separate thermodynamic signatures of a first-order liquid–liquid transition from other phenomena such as nonequilibrium kinetic limitations, crystallization, or polymerization. The scarce liquid–liquid transitions reported in the literature are based on a transition obtained by cooling a liquid. For instance, upon quenching supercooled Al<sub>2</sub>O<sub>3</sub>–Y<sub>2</sub>O<sub>3</sub> liquids, droplets of a second liquid of identical composition spontaneously appear within the liquid matrix, which is interpreted to be due to the presence of a metastable low-density/high-density liquid–liquid coexistence line.<sup>18</sup> In the case of the molecular liquid triphenyl phosphite (TPP), it is disputed whether the “glacial” phase, which evolves upon rapid

quenching of liquid I to  $\sim 220$  K, is indeed the glassy phase of liquid II or rather a defect-ordered phase, a plastic crystal, or a micro/nanocrystalline phase.<sup>19</sup> A true liquid–liquid phase transition in a molecular liquid has probably been observed in mixtures of toluene or aniline with TPP.<sup>20</sup> These transitions from liquid I to liquid II cannot be reversed, for example, because liquid II (or its glassy counterpart) crystallizes upon reheating, as, for example, for *trans*-1,2-dichloroethylene.<sup>21</sup> No direct evidence has been reported for a density-driven first-order liquid–liquid transition obtained upon (de)pressurization. Hints for the existence of such transitions such as the occurrence of a maximum in the melting temperature have been reported though. This maximum was reported at 5.6 GPa for carbon<sup>22</sup> and at 50 GPa for nitrogen.<sup>23</sup> In liquid phosphorus, a pressure maximum of the melting temperature close to 1 GPa has been confirmed by in situ diffraction experiments to be due to a first-order liquid–liquid transition associated with a 40% density change.<sup>18,24</sup> However, the high-pressure liquid involved in these transitions is a polymeric species

**Special Issue:** H. Eugene Stanley Festschrift

**Received:** April 29, 2011

**Revised:** July 12, 2011

**Published:** July 27, 2011

rather than a molecular/atomic species. In the case of interfacial Vycor hydration water<sup>25,26</sup> and water confined to the interior of protein crystals,<sup>27</sup> some evidence for a liquid–liquid transition was collected recently. It is reported that there is a dynamic crossover (fragile-to-strong) upon cooling such liquids.<sup>28,29</sup> In the case of bulk water, polyamorphic nonequilibrium transitions have been reported,<sup>6–10,30–33</sup> and it is widely believed that the liquid–liquid transition is a “virtual” transition hidden by crystallization, which cannot be observed experimentally.<sup>19</sup> Therefore, a first-order transition involving an equilibrated ultraviscous liquid state has not been reported so far.

Instead, a first-order like transition between low- (LDA) and high-density amorphous ice (HDA) is discussed.<sup>6,34</sup> Ambient pressure studies on the temperature-controlled HDA → LDA transition show two conflicting scenarios; neutron and X-ray diffraction (XRD) measurements show a continuous process from HDA to LDA, involving an infinite number of amorphous states of intermediate density.<sup>12,14,15,35,36</sup> By contrast, Raman measurements and visual observations by Mishima and Suzuki<sup>37</sup> show the propagation of a sharp phase boundary and a region containing a mixture of both ices, that is, a discontinuous transition. Please note that the HDA → LDA transition at ambient pressure represents a kinetically driven irreversible process from an unstable state to a metastable state. In order to probe the reversible (quasi-) equilibrium process between metastable LDA and metastable HDA, in situ studies are necessary. The first-order-like transition between LDA and HDA was reported on the basis of a sharp change in volume and reversibility with hysteresis using in situ experiments at high pressure.<sup>6–11</sup> The equilibrium phase boundary between metastable LDA and HDA was estimated by Whalley et al.<sup>38</sup> to be at  $\sim 0.2$  GPa. The first in situ observation of a sharp boundary between LDA and HDA was reported by Mishima et al.<sup>39</sup> using a diamond anvil cell. Further in situ studies on the transition between LDA and HDA under pressure were performed by Klotz et al.<sup>8</sup> using the Paris–Edinburgh high-pressure cell in conjunction with neutron diffraction. The authors showed that the intermediate diffraction pattern can be decomposed into a linear combination of the patterns of pure LDA and HDA. This two-state model was criticized for not being clear evidence for coexistence by Tulk et al.<sup>35</sup> However, Raman spectra were also interpreted in favor of a mixture of HDA and LDA and a first-order-like transition between LDA and HDA under pressure.<sup>8,10,11</sup>

Relaxation effects play a key role in understanding the metastable noncrystalline states and their transformations, most notably in separating mere strain relaxation processes from (polyamorphic) structural transitions overcoming potential energy barriers. It is, therefore, essential to know and control the relaxation state, in particular, of HDA states. This issue was not considered in many amorphous ice studies in the past and is certainly a source of confusion inherent to the current debate about the nature of the amorphous–amorphous transitions in water. Seminal work on the relaxation issue by Nelmes et al.<sup>9</sup> and Salzmann et al.<sup>40</sup> studied the influence of annealing of HDA at different pressures, which results in several high-density amorphous states of distinct density. Recently, Nelmes et al. suggested to call the state produced by pressure-induced amorphization of hexagonal ice at liquid nitrogen temperature (77 K) “unannealed HDA” (uHDA)<sup>9,41</sup> and characterized it as a highly strained, unrelaxed form of HDA. Annealing of uHDA at low pressures drives this amorphous state closer to the metastable equilibrium. Annealing at  $p > 0.8$  GPa to  $T \approx 160$  K causes further

densification and the formation of VHDA.<sup>42</sup> Several HDA and VHDA substates can be prepared experimentally both under high pressure and at ambient pressure, which are of higher density at  $p > 0.3$  GPa and called relaxed HDA (rHDA) by Salzmann et al.<sup>40</sup> and of lower density at  $p \leq 0.2$  GPa and called expanded HDA (eHDA) by Nelmes et al.<sup>9,34,43</sup>

Here, we probe the state of relaxation of the high-density amorph (HDA) of water at 140 K as a function of pressure and show that it can be driven to the well-relaxed state and metastable equilibrium at  $p < 0.2$  GPa. Upon decompression, HDA sharply transforms to the low-density form, where both phases are shown to segregate spatially. This phenomenology is rationalized in the framework of a density-driven first-order phase transition, where low-density clusters nucleate statistically in the high-density matrix and progressively drive a phase-boundary through the whole sample.

## EXPERIMENTAL SECTION

We used the sample preparation method described previously in our recent study.<sup>32</sup> In brief, 300  $\mu\text{L}$  of deionized  $\text{H}_2\text{O}$  was pipetted into a piston cylinder apparatus of 8 or 10 mm bore diameter kept at 77 K, thereby producing hexagonal ice. To avoid sudden pressure drops during compression, all samples were kept in a container made of  $\sim 300$  mg of thin indium foil. Hexagonal ice was then pressurized at  $T = 77$  K. When the pressure exceeded  $p \approx 1.0$  GPa hexagonal ice amorphized and formed uHDA.<sup>41</sup> VHDA was then produced by isobarically annealing uHDA at  $p \approx 1.1$  GPa to  $T \approx 160$  K<sup>42</sup> and subsequently cooled to 140 K, which served as the starting point of the decompression. VHDA was decompressed at a controlled rate of 20 MPa/min at a constant temperature of 140 K to different pressures and quenched, that is, kinetically arrested, by immersing in liquid nitrogen before recovering to ambient pressure. The recovered samples were then transferred under liquid nitrogen (at 77 K) to the XRD chamber and/or the calorimeter.

Powder X-ray diffractograms were recorded at  $\sim 80$  K on a diffractometer in  $\theta/\theta$  arrangement (Siemens, model D 5000, Cu  $K\alpha$ ), equipped with a low-temperature camera of Anton Paar. A differential scanning calorimeter (Perkin-Elmer, model DSC-4) calibrated using cyclopentane with a self-written computer program was used. DSC scans were recorded upon heating with a rate of 10 K/min from 93 to 253 K using stainless steel DSC capsules with screwable lids. As reported in ref 44, after heating each sample up to 253 K, a second heating scan of now ice Ih was recorded and subtracted as the baseline from the first scan. The mass of the sample could not be determined by weighing because filling and closing of the capsule takes place under liquid nitrogen. Instead, the sample mass was calculated from the melting endotherm of ice, using the value of 6.012 kJ/mol as the heat of melting, and typically amounted to a few mg.<sup>45</sup> All thermograms were normalized to 1 mol. The thermograms show two exotherms in the range of 100–170 K caused by the HDA → LDA and the LDA → cubic ice transformations. We extracted the initial temperature  $T_i$ , the extrapolated peak onset temperature  $T_e$  (according to refs 46–48), and the peak minimum  $T_{\text{min}}$  from the HDA → LDA exotherm. The initial temperature  $T_i$  is the temperature where the slope deviates from linearity. The extrapolated peak onset temperature is determined by the crossing of the extrapolated baseline with the tangent on the low-temperature side of the sharp exotherm.



**Figure 1.** The  $\text{H}_2\text{O}$  sample with a volume of 1.5 mL was made by decompression of VHDA at 140 K to 0.07 GPa with a rate of 13 MPa/min and quench-recovered to 77 K and 1 bar (top image). After removal from the piston cylinder apparatus, the sample easily broke into two pieces; the top fraction was placed on the left side, and the bottom piece was placed on the right side at 77 K (second from top). The bottom images shows the two pieces upon heating at ambient pressure, demonstrating the spatial segregation into a low- and high-density fraction and a phase boundary in between.

The difference between  $T_i$  and  $T_e$  is small for well-relaxed samples, whereas it is large for barely relaxed samples, in which a broad relaxation exotherm precedes the sharp exotherm caused by the latent heat of the structural transformation.

## RESULTS

**First-Order-Like Transition HDA  $\rightarrow$  LDA.** We have recently studied structural transitions in amorphous ices by decompressing VHDA at 140 K.<sup>32</sup> Eleven different quench recovered samples, kinetically arrested at different pressures, were investigated by powder XRD. The downstroke HDA  $\rightarrow$  LDA transition takes place at  $\sim 0.06$  GPa and is quasi-discontinuous, as revealed before by Mishima et al.<sup>7</sup> Our study furthermore showed that VHDA

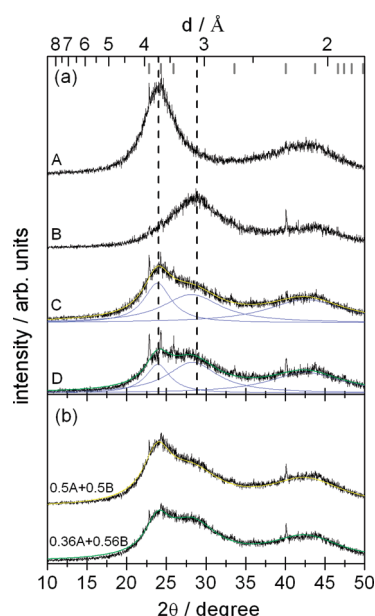


**Figure 2.** A sample of 700  $\mu\text{L}$  ( $\text{D}_2\text{O}$ ) was made by decompression of VHDA at 143 K<sup>33</sup> to 0.07 GPa with a rate of 13 MPa/min. (a) Four diffractograms taken from different parts of this sample (A: bottom, B: top, C: phase boundary, D: phase boundary). Vertical lines indicate the positions of the first broad halo peak for LDA and eHDA. Diffractograms are offset for clarity but not smoothed and not scaled. Relative intensities differ because of differing amounts of sample in the X-ray beam. Diffractograms C and D are fitted with three Lorentz functions. The single Lorentz functions are plotted in blue, and the overall fit functions are yellow and green. In part (b), these functions are plotted again for comparison. (b) Two different linear combinations of the diffractograms A(LDA) and B(eHDA). The fit function of the originally measured data also fits the linear combination of the two states LDA and eHDA. Note: Because the mass of the sample actually exposed to the beam is unknown, intensities cannot be normalized. Therefore, the sum of the two coefficients in the linear combination does not need to equal unity.

decompressed to 0.06 GPa at 140 K can result in the formation of eHDA or LDA (green diffractograms in Figure 3a of ref 32). In Figure 1, we now demonstrate that a VHDA sample decompressed to 0.07 GPa at 140 K is not homogeneous but heterogeneous. After quench-recovery, such cylindrical samples easily break into two pieces when touching them with tweezers. This behavior is in stark contrast to the behavior that we observe for amorphous samples quench-recovered from other ( $p, T$ ) points. The area of easy rupture is visible in the top image in Figure 1 as a white line close to the middle of the sample cylinder. In the second image from the top, we have placed the two separated pieces on a copper block kept at 77 K. As the picture sequence shows, the two sample parts do not behave alike upon heating at ambient pressure. The third image in Figure 1 shows that one piece, namely, the bottom piece (left), has popped up, that is, transformed from a high-density form to a low-density form. The density of the other piece (right) is unaffected at the same time. The final picture taken at even higher temperature shows the same qualitative picture, except for a slight swelling of the sample close to the area of rupture. The piece at the right side remains at the same density when heated. That is, the original cylindrical sample is a macroscopically segregated mixture of a high-density part and a low-density part and easily breaks where low-density and high-density parts abut. We observed this type of behavior

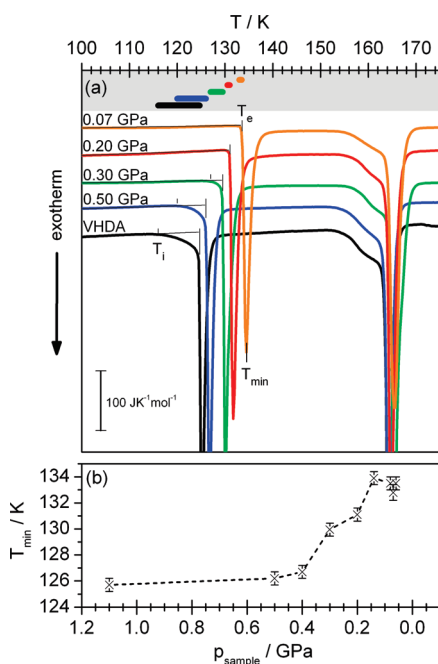


**Figure 3.** (a) DSC scans recorded at a rate of 10 K/min. The DSC output signal was normalized to 1 mol. The samples were heated from 93 to 253 K; thermograms are plotted in the temperature range of 100–175 K. Shown are VHDA (black line) and four samples made by decompression of VHDA at 140 K to 0.5 (blue line), 0.3 (green line), 0.2 (red line), and 0.07 GPa (orange line). First exothermic peak: transition to LDA; second exothermic peak: crystallization to cubic ice. The bars in the top part indicate the difference between  $T_i$  and  $T_e$  (see text), which is a measure of the relaxation state of the sample. (b) The temperature at the peak minimum  $T_{min}$  is shown as a function of the pressure from which the sample has been recovered. The values are not only obtained from the four selected runs depicted in (a) but represent mean values obtained from several runs.

for several samples decompressed to the pressure range of 0.07–0.06 GPa.

Powder X-ray diffractograms from another sample, produced in the same way, demonstrate that one piece is eHDA with a diffraction maximum at  $2\theta = 28.8^\circ$  ( $d = 3.10$  Å) (trace B in Figure 2a), whereas the other piece is LDA with a first diffraction maximum at  $2\theta = 24.0^\circ$  ( $d = 3.71$  Å) (trace A in Figure 2a). In some experiments, the bottom piece consists mainly of eHDA, and the top piece consists mainly of LDA, whereas in other experiments, it is the other way around.<sup>49</sup> LDA formed on top and bottom of the sample with eHDA sandwiched in the middle was observed only once. That is, LDA grows at random either from the bottom up or from the top down within the high-density sample. Temperature gradients and/or pressure gradients in the sample can be excluded as the origin of the observation of macroscopic segregation. If such gradients were at the origin, then the LDA fraction would always be observed at the same place rather than randomly. However, a small temperature gradient develops as a result of the latent heat released by the first-order transition in the aftermath.

The area of rupture consists of a mixture of eHDA and LDA (traces C and D in Figure 2a), as shown by an XRD analysis of small chips from the site of fracture. The “contamination” of the LDA piece by eHDA in the area of rupture is evident in the bottom image in Figure 1, where the eHDA traces in the area of rupture

have popped up and transformed to LDA. The diffractograms C and D show a double-peaked powder pattern with two maxima at  $2\theta = 24.0$  and  $28.8^\circ$ . Their shape can be fitted with three Lorentz functions (blue lines) with maxima at  $2\theta = 23.9$ ,  $28.3$ , and  $42.5^\circ$ . The overall fit function is plotted in yellow (pattern C) and green (pattern D). These double-peaked powder patterns can be produced by a linear combination of the powder pattern of LDA (A) and eHDA (B). The upper diffractogram in Figure 2b has been produced by the addition of 0.5 times diffractogram A and 0.5 times diffractogram B (0.50A + 0.50B). To show that this superposition is identical (within experimental error) to diffractogram C, also the fit function of C (yellow) is plotted. The lower diffractogram in Figure 2b has been produced by the linear combination (0.36A + 0.56B). For comparison, the fit function of diffractogram D (green) is also plotted. The diffractograms taken from the boundary area can be expressed as a superposition of the pure LDA and eHDA patterns. That is, the coexistence of eHDA and LDA is demonstrated here by XRD. This XRD analysis of the HDA  $\rightarrow$  LDA transition upon decompression shows the same picture of HDA/LDA coexistence also seen for the LDA  $\rightarrow$  HDA transformation investigated by neutron diffraction.<sup>8</sup> This is a necessary but not sufficient condition for a first-order transition. However, the additional observation of the area of rupture as a well-defined boundary between LDA and eHDA cannot be explained in the framework of a continuous transition but only by a first-order transition.

**eHDA: An Equilibrated State.** “It is eHDA and not VHDA that is relevant to the nature of the transition from LDA and the issue of the proposed second critical point” was stated by Nelmes et al.<sup>9</sup> In Figure 1, we show that indeed a macroscopic separation between eHDA(0.06 GPa) and LDA can be observed. In the following, we will discuss why eHDA is the most equilibrated HDA state observed so far and thus the only possible HDA substate that can experience a first-order transition to LDA. In our recent XRD study, we have shown the downstroke VHDA  $\rightarrow$  eHDA transition to be continuous, with eHDA as the limiting structure at the low-pressure end.<sup>32</sup> We here show with differential scanning calorimetry (DSC) that not only the structural states but also the thermal behavior evolve continuously from VHDA to eHDA upon decompression at 140 K. Some of the DSC data presented here and the XRD measurements shown in our ref 32 are taken from identical samples; some others are taken from samples prepared in the same way.

DSC scans of several HDA states are shown in Figure 3a. All samples were heated in the calorimeter with a rate of 10 K/min at 1 bar. The black scan shows the thermogram of VHDA prepared by heating uHDA at 1.1 GPa to 160 K. Lines colored blue, green, red, and orange show DSC scans of four samples made by decompression of VHDA at 140 K to 0.5, 0.3, 0.2, and 0.07 GPa (called eHDA), respectively. All thermograms show two exotherms in the range of 100–170 K caused by the HDA  $\rightarrow$  LDA and the LDA  $\rightarrow$  cubic ice transformations. The crystallization to cubic ice (second exotherm) takes place at  $T_{min} = 164 \pm 1$  K for all samples studied here. By contrast, the temperature for the amorphous–amorphous transition (first exotherm) varies from  $T_{min} \approx 117$  K for uHDA (see Figure 4c) to  $T_{min} \approx 134$  K for eHDA. This variation in  $T_{min}$  indicates different levels of relaxation, where more relaxed samples show higher  $T_{min}$ .

eHDA shows the highest thermal stability of all investigated amorphous ices, whereas uHDA shows the lowest. That is, uHDA is indeed a highly unrelaxed state far away from the metastable equilibrium in the HDA megabasin, whereas eHDA is well-equilibrated.

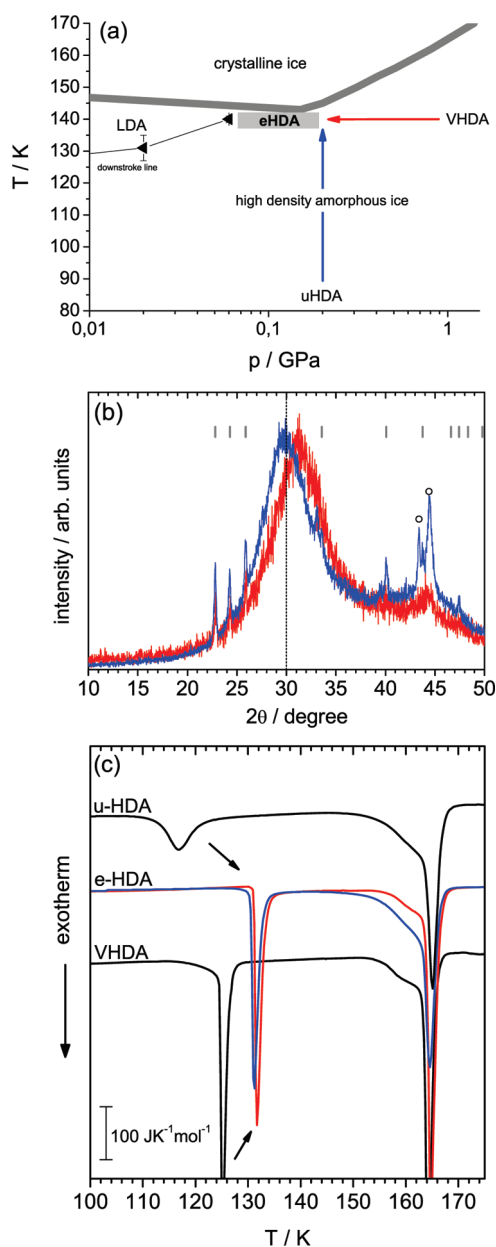


**Figure 4.** (a) Phase diagram of amorphous water in the pressure range of 0.01–1.1 GPa, with a logarithmic pressure axis. The gray line represents the crystallization temperature ( $T_X$ ) (adapted from refs 7 and 40). The HDA  $\rightarrow$  LDA downstroke transition<sup>7</sup> is shown as a black line, and the data points (black triangles) are taken from our own decompression measurements.<sup>33</sup> Red arrow: decompression of VHDA at 140 K to 0.2 GPa. Blue arrow: annealing of uHDA at 0.2 GPa to 140 K. The two distinct routes lead to the formation of a very similar HDA state. The X-ray patterns of the two HDA samples are shown in (b). Gray ticks mark the position of Ih reflections, which had formed by condensation of water vapor during transfer of the sample. Additional reflections originate from the sample holder (open circles). The corresponding DSC scans are plotted in (c). Red line: sample obtained by decompression (the DSC trace is identical to Figure 3a). Blue line: sample obtained by annealing. For comparison, the DSC traces of uHDA and VHDA (black lines) are also shown.

This large difference in thermal stability is observed, even though the structure factors determined for eHDA and uHDA are highly similar.<sup>50</sup> In the case of VHDA  $\rightarrow$  LDA, the peak minimum

appears to be at  $T_{\min} \approx 126$  K (black line), which lies inbetween the transition temperatures of uHDA  $\rightarrow$  LDA and eHDA  $\rightarrow$  LDA. However, the structure factors for VHDA and uHDA are also quite different.<sup>51</sup> This shift in thermal stability between uHDA, VHDA, and eHDA was already observed in previous studies using different experimental methods.<sup>9,52,53</sup> The transition temperature of eHDA (0.07 GPa) at  $T_{\min} \approx 134$  K is 17 K higher compared to unannealed HDA and therefore the highest transition temperature observed so far. In addition to  $T_{\min}$ , also the extrapolated peak onset temperature  $T_e$  and the initial temperature  $T_i$  are important information, which can be extracted from DSC scans (see Experimental Section above). A broad and shallow exotherm between  $T_i$  and  $T_e$  preceding a sharp, symmetric exotherm is usually regarded as the slow, continuous relaxation of strain prior to an activated transition. This type of behavior was noted by Handa et al.<sup>46</sup> for the case of uHDA and attributed to a two-stage process, first, “a slow annealing of uHDA toward a less dense form” and, second, a sharp peak indicating the irreversible transformation to LDA (transition temperature at  $\sim 114$  K<sup>46</sup>). This two-stage transformation scenario is consistent with X-ray and neutron diffraction results,<sup>12,14,36</sup> as well as ultrasonic studies.<sup>54</sup> Also, our own DSC measurements show this two-stage process. The thermogram of uHDA shows a broad and weak exotherm, extending from  $T_i \approx 108$  K to somewhere within the phase transition (sharp exotherm with  $T_{\min} \approx 117$  K), as displayed in ref 50. (Note that we do not observe a relaxation process at temperatures below 105 K, as reported by Handa et al.<sup>46</sup> This may be attributed to the fact that our calorimeter cannot be cooled below 88 K. This means that during sample transfer, the sample heats up to  $T > 90$  K, temperatures where the relaxation process is already in progress. Furthermore, we heat up with a rate of 10 K/min, which is faster compared to the calorimetry measurements by Handa et al. (10 K/h).<sup>46</sup> Nevertheless, our data totally agree with the described two-stage transformation scenario.)

Different studies on the VHDA  $\rightarrow$  LDA transition at ambient pressure show transient HDA-like states (e.g., neutron scattering<sup>55</sup> or NMR<sup>53</sup> or Raman spectroscopy<sup>37</sup>). That is, upon warming VHDA, a two-stage process is also observed; first, VHDA slowly transforms to HDA-like states, which is followed by the sharp transition to LDA. The thermogram of VHDA (black line, Figure 3a) shows, similar to the thermogram of uHDA, a broad and shallow relaxation exotherm extending from  $T_i \approx 116$  K followed by the sharp exotherm at  $T_{\min} \approx 126$  K. The temperature range of the broad exothermic relaxation process is indicated by the bar in the upper part of Figure 3a. The extrapolated peak onset temperature  $T_e$  of the sharp phase transition to LDA appears to be at  $T_e \approx 125$  K. Therefore, a transition from VHDA to a HDA-like state takes place between 116 and 125 K (black bar). A sharp exotherm for the VHDA  $\rightarrow$  HDA transition is not expected because VHDA is an unstable state at 1 bar (see Figure 8 in ref 50). This unstable state relaxes toward the metastable equilibrium state (eHDA) as long as the temperature is high enough to overcome the barrier to LDA. It never reaches the metastable equilibrium state at 1 bar within the few minutes of a calorimetry experiment, and therefore, a HDA-like state finally transforms to LDA. The nature of this HDA-like state depends on the preparation history of the sample, and therefore, VHDA or HDA samples of different relaxation level show different  $T_{\min}$  for the HDA-like  $\rightarrow$  LDA transition.

We observe an increasing thermal stability with decreasing recovery pressure for VHDA samples after decompression at

140 K and quench-recovery ( $T_{\min}$  increases; see Figure 3a and b). Additionally, the initially broad and shallow relaxation exotherm progressively narrows and finally disappears as the recovery pressure is reduced (difference between  $T_i$  and  $T_e$  goes to 0; see Figure 3a). Both observations clearly imply that the amorphous ice sample reaches a more and more relaxed state as it is decompressed at 140 K. A sample decompressed to 0.5 GPa (blue line) has a very similar structure compared to that of VHDA (see XRD pattern in ref 32). The initial temperature is shifted to  $T_i \approx 120$  K (blue line), and the sharp exotherm is observed at  $T_e \approx 126$  K. The intermediate HDA state recovered from 0.3 GPa shows an initial temperature of  $T_i \approx 127$  K (green line) and  $T_e \approx 129.5$  K. The relaxation process already takes place in the narrow window of  $\sim 2.5$  K. For the eHDA samples recovered from 0.2 (red line) and 0.07 GPa (orange line),  $T_i$  and  $T_e$  are very close together, and the recovered samples already occupy a substate close to the potential energy minimum. Judging from the highest  $T_{\min}$ , the sample recovered from 0.07 GPa is closest to the metastable equilibrium. Judging from the difference in  $T_i$  and  $T_e$  samples recovered from 0.20 and 0.07 GPa but not from 0.30 GPa or higher can be regarded as well-relaxed. A detailed discussion of the DSC data follows in a separate paper.<sup>56</sup>

In order to affirm this claim of equilibrated nature at 0.07–0.20 GPa, we have checked whether the same structural and thermal state can be prepared independent of the thermodynamic path and the time taken to reach a specific point in the phase diagram defined by pressure and temperature. To this end, we have prepared HDA at 0.20 GPa by two different routes (as depicted in Figure 4a), namely, by isobaric heating of uHDA to 140 K and 0.20 GPa (blue arrow) and by isothermal decompression of VHDA to 0.20 GPa at 140 K (red arrow).

Both samples show similar but not identical powder X-ray diffractograms (Figure 4b). The diffractogram of uHDA shows a first broad maximum at  $d \approx 3.00$  Å;<sup>41</sup> the pattern after annealing uHDA at 0.2 GPa to 140 K, and subsequently quenching the sample, shows the maximum at  $d = 2.97$  Å (blue pattern in Figure 4b,  $2\theta = 30.1 \pm 0.2^\circ$ ), that is, the structure of the sample did not change within experimental error. The thermal behavior instead changes dramatically. The transition temperature for the HDA  $\rightarrow$  LDA transitions shifts from  $T_{\min} \approx 117$  K for the uHDA case (black trace, Figure 4c) to  $\sim 131.2$  K for the annealed sample (blue trace, Figure 4c). As shown in our recent study,<sup>32</sup> the X-ray diffractogram of VHDA decompressed at 140 K to 0.2 GPa shows a first broad diffraction maximum at  $2\theta = 30.8^\circ$  (red pattern in Figure 4b), which lies in between VHDA ( $2\theta = 32.3^\circ$ ) and uHDA ( $2\theta = 30.0^\circ$ ). The DSC trace of this state, called eHDA(0.2 GPa), is plotted in red in Figure 3a as well as in Figure 4c. The minimum temperature is  $T_{\min} = 131.4 \pm 0.5$  K (mean value of four batches). That is, the two samples show nearly identical DSC traces, even though the route of preparation is entirely different.

Hence, we do indeed work in the metastable equilibrium at 140 K and  $p \lesssim 0.20$  GPa. The assignment of ergodicity at 140 K for  $p \lesssim 0.2$  GPa is consistent with our recent study of the volumetric glass-to-liquid transition onset temperature  $T_{g,\text{onset}}$  for HDA samples, in which we determined  $T_{g,\text{onset}}(\text{HDA}, 0.1 \text{ GPa}) \approx 134 \pm 2$  K,  $T_{g,\text{onset}}(\text{HDA}, 0.2 \text{ GPa}) \approx 140 \pm 2$  K, and  $T_{g,\text{onset}}(\text{HDA}, 0.3 \text{ GPa}) \approx 142 \pm 2$  K.<sup>57</sup> In other words, a sample temperature of 140 K implies glassy nature at  $p > 0.2$  GPa and a transition from glass to liquid at  $p \lesssim 0.2$  GPa.

## DISCUSSION AND CONCLUSIONS

The results presented here show that eHDA, the HDA state that transforms directly to LDA,<sup>9</sup> is a well-equilibrated state. Calorimetry measurements of different recovered states, obtained upon decompressing VHDA at 140 K, show an increase in the thermal stability toward transformation to LDA as the recovery pressure is reduced. In addition, the broad and shallow structural relaxation exotherm preceding the transformation to LDA disappears as the recovery pressure is reduced. The transition temperatures ( $T_{\min}$ ) at ambient pressure increases from  $\sim 117$  K for the uHDA  $\rightarrow$  LDA transition to  $\sim 126$  K for the VHDA  $\rightarrow$  LDA transition and to  $\sim 134$  K for the eHDA  $\rightarrow$  LDA transition. The calorimetry measurements are in line with other experiments<sup>37,53,55</sup> showing that VHDA transforms at ambient pressure to HDA-like states before it converts to the low-density form. The fact that eHDA(0.07 GPa) transforms directly to LDA, without showing a preceding relaxation process, at the highest transformation temperature observed so far, is a strong hint for being a fully relaxed and thus equilibrated state. Mishima has already demonstrated an increase in thermal stability by DTA measurements on HDA samples heated (or annealed) at high pressures or amorphized at high temperatures.<sup>52</sup> The present study shows that annealing at low pressures or decompression at high temperatures causes a further increase of the thermal stability. Annealing of uHDA at 0.2 GPa to 140 K produces a very similar HDA state as decompression of VHDA to 0.2 GPa at 140 K. That is, at 140 K, we work in the metastable equilibrium and  $p \lesssim 0.20$  GPa, but we work in the nonequilibrium at higher pressure.

The results presented in Figures 1 and 2 are consistent with a first-order transition eHDA  $\rightarrow$  LDA as postulated by Mishima et al.<sup>6</sup> and recently advocated by Klotz et al.<sup>8</sup> and Yoshimura et al.<sup>10</sup> Going beyond these studies, our results also show macroscopic separation of eHDA and LDA in one single sample. That is evidenced by visual observation (Figure 1) and XRD (Figure 2). The decompression procedure produces macroscopically segregated disordered “phases” of low and high density at  $\sim 0.06$  GPa. The double-peaked powder pattern obtained by XRD and the fact that they can be reproduced by superposition of the LDA and eHDA diffractograms confirm the neutron diffraction data by Klotz et al.<sup>8</sup> Using a cylindrical pressure vessel with uniaxially applied force, we rule out the effect of pressure and/or temperature gradients to be responsible for this effect also because the transformation takes places randomly in the sample volume. The direction of propagation can be either from the bottom up or from the top down, or even in both directions.

In LDA, the glass-to-liquid transition to LDL was observed calorimetrically at ambient pressure as an endothermic event at  $T_g = 136 \pm 2$  K at a heating rate of 30 K/min.<sup>44,58</sup> The dielectric relaxation time of ultraviscous low-density water at ambient pressure is estimated to be  $\sim 30$  s at  $\sim 140$  K.<sup>59,60</sup> The liquid nature of the sample is also consistent with the penetration of a blunted conical indenter into a sample of LDA at  $T \approx 136$  K<sup>61</sup> and significant isotope exchange in films kept at  $T > 136$  K.<sup>62</sup> Because  $T_g \approx 136$  K for LDA samples at 1 bar is expected to be relatively insensitive to pressure changes,<sup>63</sup> we assume ultraviscous liquid character (LDL) for the low-density fraction of the sample at 0.07 GPa and 140 K. Furthermore, this work shows uHDA to be a highly unrelaxed state far away from the metastable equilibrium in the HDA megabasin, whereas eHDA is well-equilibrated. A recent study done by our group shows the glass transition onset temperature in HDA to be  $< 140$  K at  $p < 0.2$  GPa.<sup>57</sup>

We, thus, regard eHDA at 0.07 GPa and 140 K to be in an ultraviscous liquid state. Therefore, we suggest that the sudden macroscopic phase separation at 0.07 GPa and 140 K represents the observation of a first-order transition between an ultraviscous high-density bulk liquid (HDL) and an ultraviscous low-density bulk liquid (LDL). We rationalize the phenomenology in terms of low-density liquid clusters nucleating statistically somewhere in the cylindrical high-density liquid sample during uniaxial decompression at  $p \approx 0.07$  GPa. These low-density liquid clusters grow, and a LDL–HDL phase boundary propagates through the cylinder in the pressure range between 0.07 and 0.06 GPa. At  $p \approx 0.05$  GPa, the whole HDL sample has transformed to LDL. This interpretation is speculative because we cannot observe the nucleation and growth process directly under pressure at 140 K with our equipment. However, the results presented provide good evidence that the isothermal high- to low-density transition at 140 K takes place in the domain of “ultraviscous water”. The finding supports the scenario of a first-order liquid–liquid transition in bulk water.<sup>4</sup>

## ■ ASSOCIATED CONTENT

**S Supporting Information.** A movie showing the picture sequence in Figure 1. This material is available free of charge via the Internet at <http://pubs.acs.org>.

## ■ AUTHOR INFORMATION

### Corresponding Author

\*E-mail: [katrin.winkel@uibk.ac.at](mailto:katrin.winkel@uibk.ac.at).

### Notes

<sup>5</sup>Deceased March 13, 2011.

## ■ ACKNOWLEDGMENT

We are grateful to H. E. Stanley, P. G. Debenedetti, O. Mishima, and J. S. Loveday for helpful discussions. We gratefully thank the Austrian Science Fund (FWF START Award Y391 to T.L. and a Hertha-Firnberg fellowship to K.W.) and the European Research Council (ERC Starting Grant SULIWA to T.L.) for financial support.

## ■ REFERENCES

- McMillan, P. F.; Wilson, M.; Wilding, M. C.; Daisenberger, D.; Mezouar, M.; Greaves, G. N. *J. Phys.: Condens. Matter* **2007**, *19*, 415101/1.
- Poole, P. H.; Sciortino, F.; Essmann, U.; Stanley, H. E. *Nature* **1992**, *360*, 324.
- Stanley, H. E. *Pramana* **1999**, *53*, 53.
- Mishima, O.; Stanley, H. E. *Nature* **1998**, *396*, 329.
- Angell, C. A.; Bressel, R. D.; Hemmati, M.; Sare, E. J.; Tucker, J. C. *Phys. Chem. Chem. Phys.* **2000**, *2*, 1559.
- Mishima, O.; Calvert, L. D.; Whalley, E. *Nature* **1985**, *314*, 76.
- Mishima, O. *J. Chem. Phys.* **1994**, *100*, 5910.
- Klotz, S.; Straessle, T.; Nelmes, R. J.; Loveday, J. S.; Hamel, G.; Rousse, G.; Canny, B.; Chervin, J. C.; Saitta, A. M. *Phys. Rev. Lett.* **2005**, *94*, 025506.
- Nelmes, R. J.; Loveday, J. S.; Straessle, T.; Bull, C. L.; Guthrie, M.; Hamel, G.; Klotz, S. *Nat. Phys.* **2006**, *2*, 414.
- Yoshimura, Y.; Stewart, S. T.; Mao, H.-K.; Hemley, R. J. *J. Chem. Phys.* **2007**, *126*, 174505.
- Yoshimura, Y.; Mao, H.; Hemley, R. J. *J. Phys.: Condens. Matter* **2007**, *19*, 425214.
- Tulk, C. A.; Benmore, C. J.; Urquidi, J.; Klug, D. D.; Neuefeind, J.; Tomberli, B.; Egelstaff, P. A. *Science* **2002**, *297*, 1320.
- Paschek, D.; Geiger, A. Characterizing the stepwise transformation from a low-density to a very-high-density form of supercooled liquid water. In *Los Alamos National Laboratory, Preprint Archive, Condens. Matter*; Los Alamos National Laboratory: Los Alamos, NM, 2005; p 1.
- Guthrie, M.; Urquidi, J.; Tulk, C. A.; Benmore, C. J.; Klug, D. D.; Neuefeind, J. *Phys. Rev. B* **2003**, *68*, 184110.
- Tse, J. S.; Klug, D. D.; Guthrie, M.; Tulk, C. A.; Benmore, C. J.; Urquidi, J. *Phys. Rev. B* **2005**, *71*, 214107.
- Strassle, T.; Klotz, S.; Hamel, G.; Koza, M. M.; Schober, H. *Phys. Rev. Lett.* **2007**, *99*, 175501/1.
- Debenedetti, P. G. *J. Phys.: Condens. Matter* **2003**, *15*, R1669.
- Katayama, Y.; Mizutani, T.; Utsumi, W.; Shimomura, O.; Yamakata, M.; Funakoshi, K.-I. *Nature* **2000**, *403*, 170.
- Tanaka, H.; Kurita, R.; Mataka, H. *Phys. Rev. Lett.* **2004**, *92*, 025701/1.
- Kurita, R.; Murata, K.-i.; Tanaka, H. *Nat. Mater.* **2008**, *7*, 647.
- Rzoska, S.; Ziolo, J.; Drozd-Rzoska, A.; Tamarit, J. L.; Veglio, N. *J. Phys.: Condens. Matter* **2008**, *20*, 244124/1.
- Brazhkin, V. V.; Lyapin, A. G. *J. Phys.: Condens. Matter* **2003**, *15*, 6059.
- Mukherjee, G. D.; Boehler, R. *Phys. Rev. Lett.* **2007**, *99*, 225701/1.
- Brazhkin, V. V.; Katayama, Y.; Inamura, Y.; Kondrin, M. V.; Lyapin, A. G.; Popova, S. V.; Voloshin, R. N. *JETP Lett.* **2003**, *78*, 393.
- Zanotti, J. M.; Bellissent-Funel, M. C.; Chen, S. H. *Europhys. Lett.* **2005**, *71*, 91.
- Zanotti, J. M.; Bellissent-Funel, M. C.; Chen, S. H.; Kolesnikov, A. I. *J. Phys.: Condens. Matter* **2006**, *18*, S2299.
- Kim, C. U.; Barstow, B.; Tate, M. W.; Gruner, S. M. *Proc. Natl. Acad. Sci. U.S.A.* **2009**, *106*, 4596.
- Faraone, A.; Liu, L.; Mou, C.-Y.; Yen, C.-W.; Chen, S.-H. *J. Chem. Phys.* **2004**, *121*, 10843.
- Chen, S. H.; Liu, L.; Fratini, E.; Baglioni, P.; Faraone, A.; Mamontov, E. *Proc. Natl. Acad. Sci. U.S.A.* **2006**, *103*, 9012.
- Loerting, T.; Schustereder, W.; Winkel, K.; Salzmann, C. G.; Kohl, I.; Mayer, E. *Phys. Rev. Lett.* **2006**, *96*, 025702.
- Winkel, K.; Schustereder, W.; Kohl, I.; Salzmann, C. G.; Mayer, E.; Loerting, T. Isothermal Amorphous–Amorphous–Amorphous Transitions in Water. In *Proc. 11th Intl. Conf. on the Physics and Chemistry of Ice*; Kuhs, W. F., Ed.; RSC: Dorchester, U.K., 2007; p 641.
- Winkel, K.; Elsaesser, M. S.; Mayer, E.; Loerting, T. *J. Chem. Phys.* **2008**, *128*, 044510/1.
- Winkel, K.; Elsaesser, M. S.; Seidl, M.; Bauer, M.; Mayer, E.; Loerting, T. *J. Phys.: Condens. Matter* **2008**, *20*, 494212.
- Mishima, O. *Proc. Jpn. Acad., Ser. B* **2010**, *86*, 165.
- Tulk, C. A.; Benmore, C. J.; Klug, D. D.; Neuefeind, J. *Phys. Rev. Lett.* **2006**, *96*, 149601/1.
- Koza, M. M.; Schober, H.; Fischer, H. E.; Hansen, T.; Fujara, F. *J. Phys.: Condens. Matter* **2003**, *15*, 321.
- Mishima, O.; Suzuki, Y. *Nature* **2002**, *419*, 599.
- Whalley, E.; Klug, D. D.; Handa, Y. P. *Nature* **1989**, *342*, 782.
- Mishima, O. *Science* **1991**, *254*, 406.
- Salzmann, C. G.; Loerting, T.; Klotz, S.; Mirwald, P. W.; Hallbrucker, A.; Mayer, E. *Phys. Chem. Chem. Phys.* **2006**, *8*, 386.
- Mishima, O.; Calvert, L. D.; Whalley, E. *Nature* **1984**, *310*, 393.
- Loerting, T.; Salzmann, C.; Kohl, I.; Mayer, E.; Hallbrucker, A. *Phys. Chem. Chem. Phys.* **2001**, *3*, 5355.
- Suzuki, Y.; Tominaga, Y. *J. Chem. Phys.* **2010**, *133*.
- Kohl, I.; Bachmann, L.; Hallbrucker, A.; Mayer, E.; Loerting, T. *Phys. Chem. Chem. Phys.* **2005**, *7*, 3210.
- Hallbrucker, A.; Mayer, E. *J. Phys. Chem.* **1987**, *91*, 503.
- Handa, Y. P.; Mishima, O.; Whalley, E. *J. Chem. Phys.* **1986**, *84*, 2766.
- Hoehne, G.; Hemminger, W.; Flammersheim, H.-J. *Differential Scanning Calorimetry*; Springer: New York, 1996.
- Salzmann, C. G.; Radaelli, P. G.; Finney, J. L.; Mayer, E. *Phys. Chem. Chem. Phys.* **2008**, *41*, 6313.

- (49) Winkel, K. Study of amorphous–amorphous transitions in water. Dissertation, University of Innsbruck, Verlag Dr. Hut, ISBN 978-3-86853-875-5; 2009.
- (50) Loerting, T.; Winkel, K.; Seidl, M.; Bauer, M.; Mitterdorfer, C.; Handle, P. H.; Salzmann, C. G.; Mayer, E.; Finney, J. L.; Bowron, D. T. *Phys. Chem. Chem. Phys.* **2011**, *13*, 8783.
- (51) Finney, J. L.; Bowron, D. T.; Soper, A. K.; Loerting, T.; Mayer, E.; Hallbrucker, A. *Phys. Rev. Lett.* **2002**, *89*, 205503.
- (52) Mishima, O. *Nature* **1996**, *384*, 546.
- (53) Scheuermann, M.; Geil, B.; Winkel, K.; Fujara, F. J. *Chem. Phys.* **2006**, *124*, 224503/1.
- (54) Gromnitskaya, E. L.; Stal'gorova, O. V.; Brazhkin, V. V.; Lyapin, A. G. *Phys. Rev. B* **2001**, *64*, 094205.
- (55) Koza, M. M.; Geil, B.; Winkel, K.; Koehler, C.; Czeschka, F.; Scheuermann, M.; Schober, H.; Hansen, T. *Phys. Rev. Lett.* **2005**, *94*, 125506.
- (56) Winkel, K.; Handle, P.; Elsaesser, M. S.; Seidl, M.; Bauer, M.; Mayer, E.; Loerting, T. In preparation.
- (57) Seidl, M.; Elsaesser, M. S.; Winkel, K.; Zifferer, G.; Mayer, E.; Loerting, T. *Phys. Rev. B* **2011**, *83*, 100201.
- (58) Johari, G. P.; Hallbrucker, A.; Mayer, E. *Nature* **1987**, *330*, 552.
- (59) Johari, G. P. *J. Chem. Phys.* **2005**, *122*, 144508.
- (60) Johari, G. P.; Andersson, O. *Thermochim. Acta* **2007**, *461*, 14.
- (61) Johari, G. P. *J. Phys. Chem. B* **1998**, *102*, 4711.
- (62) Smith, R. S.; Kay, B. D. *Nature* **1999**, *398*, 788.
- (63) Xu, L. M.; Buldyrev, S. V.; Giovambattista, N.; Angell, C. A.; Stanley, H. E. *J. Chem. Phys.* **2009**, *130*, 054505.